X-ray induced photodynamic therapy with copper-cysteamine nanoparticles in mice tumors

Samana Shrestha[a], Jing Wu[b], Bindeshwar Sah[a], Adam Vanasse[a], Leon N Cooper[c,d,1], Lun Ma[e], Gen Li[e], Huibin Zheng[e], Wei Chen[e,1], and Michael P. Antosh[a,d,1]

[a]Department of Physics, University of Rhode Island, Kingston, RI 02881; [b]Department of Computer Science and Statistics, University of Rhode Island, Kingston, RI 02881; [c]Department of Physics, Brown University, Providence, RI 02912; [d]Institute for Brain and Neural Systems, Brown University, RI 02912; and [e]Department of Physics, The University of Texas, Arlington, TX 76019

Contributed by Leon N. Cooper, June 18, 2019 (sent for review January 14, 2019; reviewed by Naomi Matsuura and Anton Naumov)

Photodynamic therapy (PDT), a treatment that uses a photosensitizer, molecular oxygen, and light to kill target cells, is a promising cancer treatment method. However, a limitation of PDT is its dependence on light that is not highly penetrating, precluding the treatment of tumors located deep in the body. Copper-cysteamine nanoparticles are a new type of photosensitizer that can generate cytotoxic singlet oxygen molecules upon activation by X-rays. In this paper, we report on the use of copper-cysteamine nanoparticles, designed to be targeted to tumors, for X-ray–induced PDT. In an in vivo study, results show a statistically significant reduction in tumor size under X-ray activation of pH-low insertion peptide–conjugated, copper-cysteamine nanoparticles in mouse tumors. This work confirms the effectiveness of copper-cysteamine nanoparticles as a photosensitizer when activated by radiation and suggests that these Cu-Cy nanoparticles may be good candidates for PDT in deeply seated tumors when combined with X-rays and conjugated to a tumor-targeting molecule.

copper-cysteamine | radiotherapy | photosensitization | nanoparticles | cancer

Photodynamic therapy (PDT) involves the use of light and a photosensitizer that induces the production of reactive oxygen species at the tumor site after the absorption of light energy to kill nearby tumor cells (1–13). Singlet oxygen has a short lifetime in biological systems, less than 0.04 μs, and therefore has a short radius of action of less than 0.02 μm (10, 14). Thus, PDT is minimally invasive, and when used with light and a photosensitizer to selectively target cancerous cells, can minimize side effects to surrounding healthy tissues (1, 2, 5, 7, 10, 15–17). PDT is also unlikely to cause genotoxicity, rarely leads to DNA damage, and is effective at treating tumors that have already developed resistance to other cytotoxic treatments such as radiotherapy, hormone therapy, or chemotherapy (10, 18–22).

Despite these advantages, one major drawback of PDT is the limited penetration depth of light. PDT agents generate reactive oxygen species after the interaction with light, and the wavelengths of light for most of the clinically approved photosensitizers are in the ultraviolet (UV)/visible range (23, 24). This limits the use of conventional PDT methods to skin (surface) tumors only, and it is not effective for deep tumors (5, 17, 25–28). Recently, possible solutions to treat deep tumors with PDT have been proposed, for example: (*i*) the use of agents activatable by near-infrared (NIR) light with relative longer wavelengths (29–38), (*ii*) the use of upconversion nanoparticles that absorb NIR light and emit visible light to activate conventional photosensitizers (39–42), (*iii*) the use of fiber optics that transmit light deep into tissue (37), and (*iv*) the use of ionizing X-rays for photosensitizer activation (27). However, NIR light with enough energy to activate photosensitizers can penetrate only 5 mm into tissue (43). Similarly, upconversion nanoparticles are also limited by the penetration depth of NIR. The use of fiber optics is invasive, inconvenient, and cannot effectively and homogenously activate the photosensitizers (44, 45). Furthermore, the treatment of metastatic sites or lymph nodes is difficult as these sites are located in regions where light delivery is challenging. In contrast, the use of X-rays to activate photosensitizers may overcome the challenges of light penetration as X-rays, already used in medical imaging and therapy, can easily penetrate as deeply as necessary into patients.

Copper-cysteamine (Cu-Cy) nanoparticles are promising photosensitizing agents that can be effectively activated by X-rays to produce singlet oxygen for efficient deep cancer treatment (46, 47). Fig. 1 shows a schematic of the use of Cu-Cy nanoparticles for X-ray–activated photodynamic therapy. In this paper, we expand on a previous pilot study to measure the survival of a large cohort of mice after X-ray activation of Cu-Cy nanoparticles in comparison with controls. In this study, Cu-Cy nanoparticles are conjugated to a pH-low insertion peptide (pHLIP) (48–51) to facilitate active targeting of these nanoparticles to low pH tumors in the future.

Results

pHLIP-Cu-Cy Nanoparticle Characterization and Assessment. As energy transfer is needed to produce singlet oxygen using X-rays, nanoparticle luminescence will occur, with stronger luminescence potentially resulting in more effective singlet oxygen production, and more efficient PDT. Cu-Cy nanoparticles exhibit strong luminescence, while many copper complexes have no luminescence due to efficient internal conversion (52, 53). Fig. 2*A* shows the Cu-Cy nanoparticles suspended in an aqueous solution, and its fluorescence under UV excitation is shown in Fig. 2*B*. The TEM image demonstrated that the average size of Cu-Cy

Significance

Copper-cysteamine nanoparticles can be activated directly by X-rays to produce singlet oxygen. The use of copper-cysteamine nanoparticles (conjugated with pH-low insertion peptide) can enhance the effects of X-ray–induced photodynamic therapy, to lead to improved tumor treatment in mice. The results of this study demonstrate the potential of copper-cysteamine nanoparticles with deeply penetrating X-rays in the treatment of mammalian cancer to overcome current limitations of low penetration, light-induced photodynamic therapy treatment that can only treat superficial cancers.

Author contributions: L.N.C., L.M., W.C., and M.P.A. designed research; S.S., B.S., A.V., and L.M. performed research; J.W. analyzed data; and J.W., G.L., H.Z., W.C., and M.P.A. wrote the paper.

Reviewers: N.M., University of Toronto; and A.N., Texas Christian University.

The authors declare no conflict of interest.

[1]To whom correspondence may be addressed. Email: leon_cooper@brown.edu, weichen@uta.edu, or mantosh@uri.edu.

This article contains supporting information online at www.pnas.org/lookup/suppl/doi:10.1073/pnas.1900502116/-/DCSupplemental.

Published online August 1, 2019.

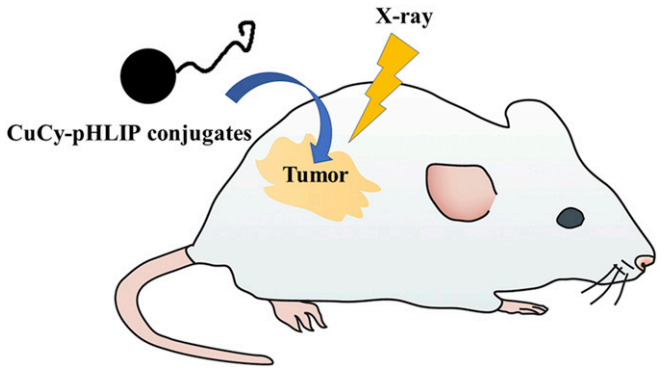

Fig. 1. A schematic illustration of X-ray–induced PDT with pHLIP-conjugated Cu-Cy nanoparticles in mice.

nanoparticles was ~200 nm. In Fig. 2*C*, the Cu-Cy nanoparticles appear to have a flake structure surrounding them, which are likely the seeds of Cu-Cy nanoparticles because Cu-Cy has a layered crystal structure, and it may form some flake-like crystal seeds. Upon excitation at 365 nm, these nanoparticles demonstrated emission in the red, peaking at 607 nm with a shoulder at 633 nm, indicating two luminescence-emitting centers (Fig. 2*D*). The luminescence of Cu-Cy corresponds to the Cu MC transition ($d^9 4s^1$–d^{10}), which can be strongly effected by Cu–Cu interactions (54). These two emission peaks from Cu-Cy are caused by two types of copper ions, Cu (1) and Cu (2), existing in the Cu-Cy nanoparticles, which are different from each other by different coordination (55).

The conjugation of poly(ethylene glycol) methyl ether thiol-coated Cu-Cy nanoparticles with pHLIP were characterized by optical absorption and luminescence spectra (56, 57). Cu-Cy nanoparticles have only red emission with doublet peaks at 606 and 636 nm. However, the PHLIP-Cu-Cy nanoparticle conjugates have two emissions in the blue and the red (*SI Appendix*, Fig. S1). The red is from Cu-Cy nanoparticles, and the blue emission at 448 nm is due to the peptides. Cu-Cy nanoparticles have a strong absorption at 360 nm (*SI Appendix*, Fig. S2). When the conjugates were excited at 360 nm, both emissions from Cu-Cy nanoparticles and the peptides are observed. When the excitation spectrum was recorded by monitoring the blue emission at 448 nm, both the excitation peaks at 280 and 360 nm were observed. This indicated there is energy transfer between Cu-Cy nanoparticles and the peptides and that the conjugation was successful.

Effect of Cu-Cy Nanoparticles on Tumor Size after Radiation Therapy. Fig. 3 and *SI Appendix*, Fig. S3 shows the average tumor volume as a function of time after irradiation. pHLIP-conjugated Cu-Cy nanoparticles produced a reduction in tumor size in both sexes, compared with mice given Cu-Cy nanoparticles (not conjugated to pHLIP) and radiation, mice given radiation only (no nanoparticles), and all nonirradiated mice. Longitudinal data analysis in the joint model (*SI Appendix*, Table S1) shows that radiation ($P = 0.0001$) and pHLIP-conjugated Cu-Cy nanoparticles ($P = 0.0386$) had significant negative effects on tumor size, indicating that both radiation therapy and pHLIP-conjugated Cu-Cy nanoparticle treatment tend to reduce the tumor size (cube root of volume) during the course of the study. In addition, the baseline tumor size ($P < 0.0001$) had a significant positive effect, meaning that mice with larger tumor sizes at the initial time point were more likely to have a larger tumor size at the later time points. The quadratic term of time effects ($P < 0.0001$) found to be significant is known to have an explicit effect on tumor size as a function of time. The effect of sex was found to be statistically insignificant ($P = 0.5091$). To control the familywise error rate (FWER = 5%) (58), a Bonferroni correction was applied (*SI Appendix*, Table S1), and the difference between radiation therapy with pHLIP-conjugated Cu-Cy nanoparticles and

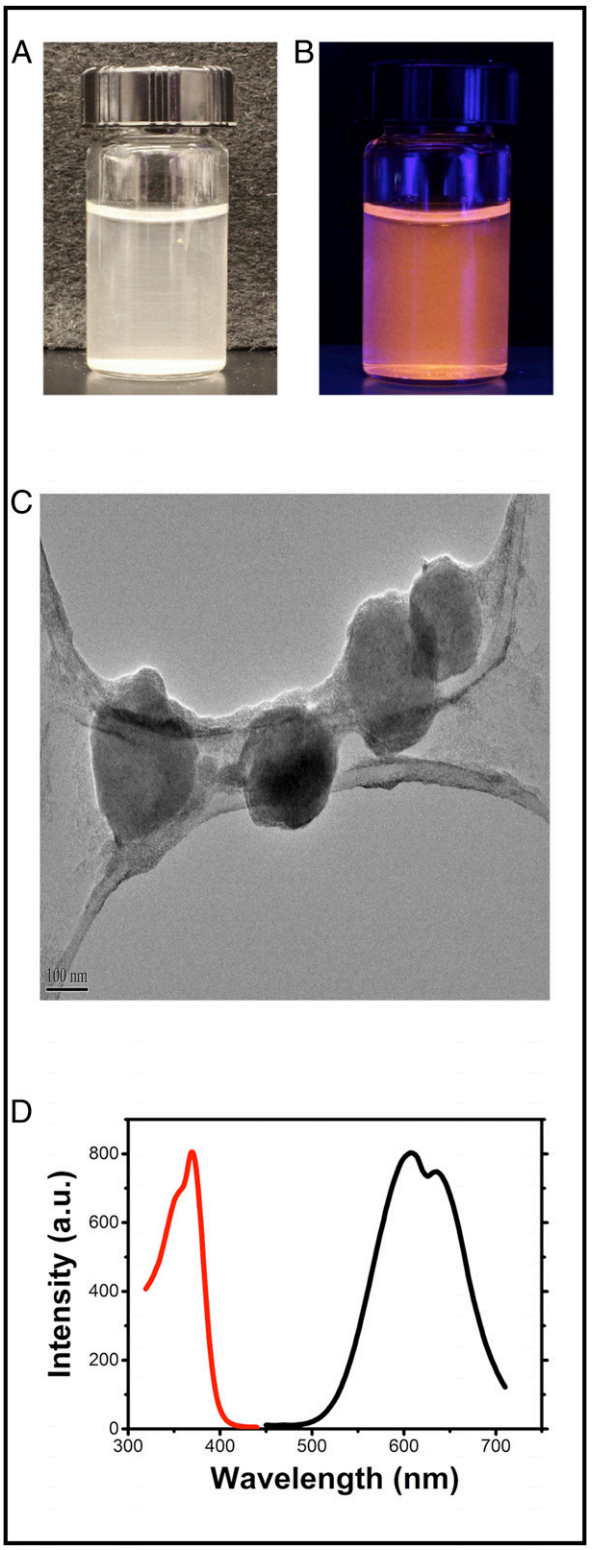

Fig. 2. A photo of the Cu-Cy nanoparticles in aqueous solution (*A*), under a UV lamp (*B*), and under TEM (*C*). (*D*) The excitation (emission at 645 nm, *Left*) and emission (excitation at 365 nm, *Right*) of Cu-Cy nanoparticles.

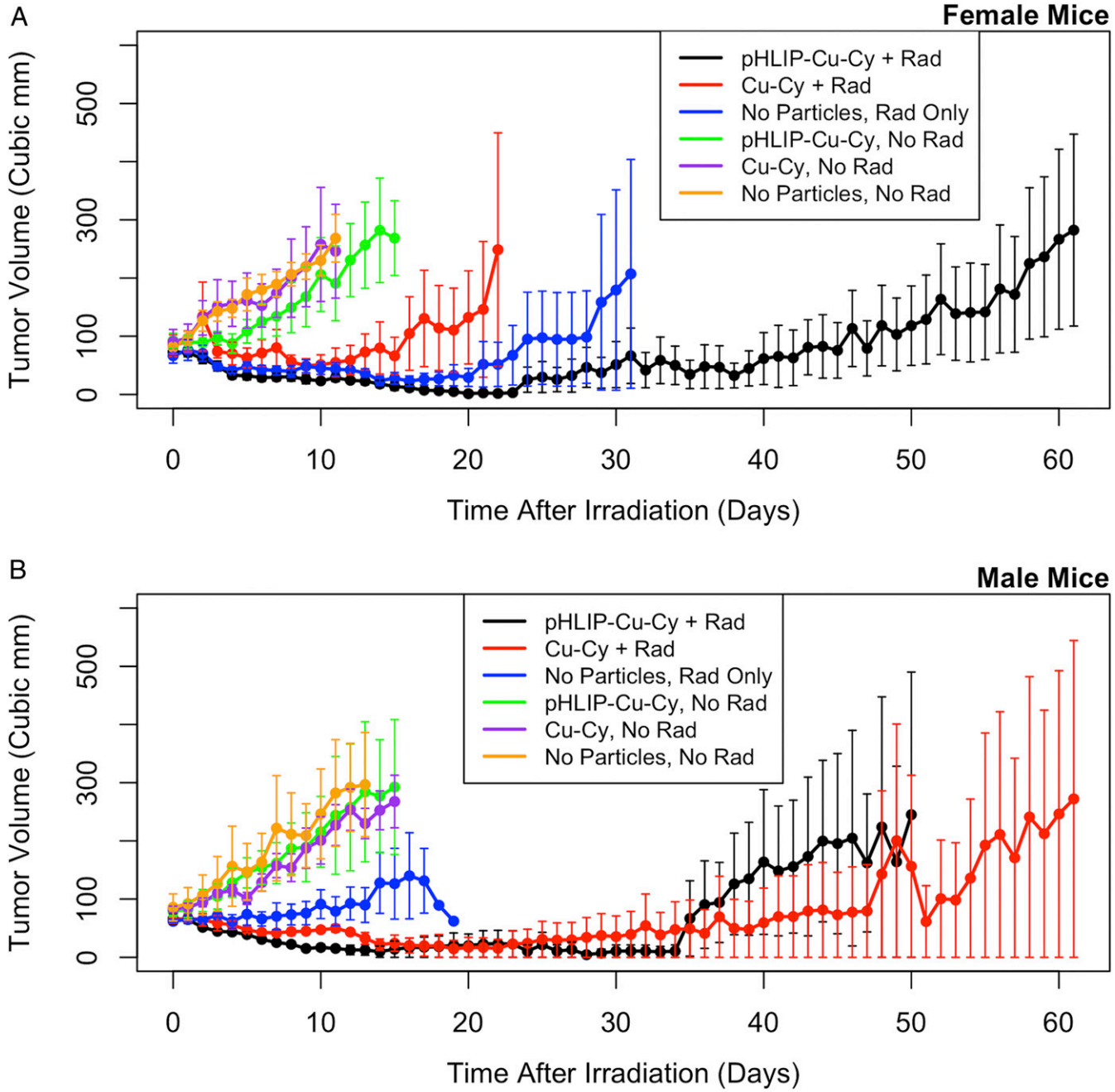

Fig. 3. Tumor size as a function of time for female (*A*) and male (*B*) mice. Treatment with pHLIP-conjugated Cu-Cy nanoparticles and radiation shows a reduction in tumor size, compared with treatments of plain Cu-Cy nanoparticles and radiation and treatments of radiation only (no nanoparticles). Mean and SEM is plotted. Curves in this figure were cut off when average tumor size reached 300 mm^3 for the first time, or when only one mouse was left alive. For the last two data points of the radiation-only mice (blue), the error bars are too small to be visible. The full dataset used in the analysis is plotted in *SI Appendix*, Fig. S3.

radiation therapy with no nanoparticles was negatively significant ($P < 0.0001$), indicating that pHLIP-conjugated Cu-Cy nanoparticles can significantly reduce the tumor size under X-ray activation compared with X-rays alone.

In contrast to the results for pHLIP-conjugated Cu-Cy nanoparticles, the difference between the treatments (radiation therapy and plain Cu-Cy nanoparticles versus radiation therapy with no nanoparticles) was not statistically significant ($P = 0.5082$). This shows that tumor size did not significantly decrease in this experiment when irradiated with plain Cu-Cy nanoparticles, suggesting a benefit from the pHLIP conjugation. Further supporting this conclusion, the difference between the treatments (radiation therapy and pHLIP-conjugated Cu-Cy nanoparticles versus radiation therapy and plain Cu-Cy nanoparticles) was statistically significant ($P < 0.0001$), with the pHLIP-conjugated nanoparticles resulting in smaller tumor sizes. The results of survival data analysis in the joint model are given in *SI Appendix*, Table S1, where no covariates were found to be significant.

Discussion

In this paper, we demonstrated that Cu-Cy nanoparticles conjugated to pHLIP can reduce tumor size when combined with radiation therapy in mice. Cu-Cy nanoparticles can be used in

the treatment of both shallow and deep tumors because it can be activated by X-rays as well as light (46, 47). Cu-Cy nanoparticles interact with X-rays and produce both fluorescence (Fig. 4*A*) and singlet oxygen (55). Singlet oxygen is a reactive oxygen species, which causes damage to cells. Fig. 4*B* shows the energy level structure of Cu-Cy nanoparticles; in particular, the intersystem crossing from S_1 to S_0 results in an energy transfer and singlet oxygen generation. The mechanism for X-ray interactions with Cu-Cy nanoparticles to produce singlet oxygen is similar to the process for light activation to produce singlet oxygen; the only difference is that the excitation with X-rays is to higher excited levels, while the relaxation to lower energy levels and the energy transfer from the triplet state to excite dioxygen to produce oxygen are the same as illustrated (Fig. 4*B*). Cu-Cy nanoparticles have been used in therapy for SW620 colorectal cancer (47) and MCF-7 cells both in vitro and in vivo (46).

pHLIP-conjugated Cu-Cy nanoparticles showed the enhanced radiation effect with improved tumor size reduction in both male and female mice. It is possible that pHLIP contributed to the enhancement effect by binding Cu-Cy directly to a cell. Singlet oxygen is known to have a short lifetime (~4 μs; refs. 59 and 60); thus, it may be of additional use to connect Cu-Cy directly to a cell. The effect of initial volume in the longitudinal analysis makes logical sense, because a tumor starting at a larger volume will have larger volumes overall than if it had started at a smaller volume. However, it is still a reminder of the importance of having mice irradiated with initial tumor volumes grouped as closely as possible.

Two particularly important variables that were not tested in this work are radiation energy and radiation dose. Few, if any, photoluminescent particles have been shown to work at energies as high as 90 kVp, which was the radiation energy spectrum applied in this work. However, most clinically relevant energies are higher. In the future, the effectiveness of higher energy photons and delivered dose will be evaluated. In addition, although this paper is about the application of PDT to deeper cancers, many skin cancers are treated with kiloelectron volt-level radiation (61), and Cu-Cy nanoparticles may be able to enhance the effectiveness of this process.

Overall, this paper demonstrates the strong potential of pHLIP-conjugated Cu-Cy nanoparticles, combined with X-rays, as a photosensitizer for PDT to successfully treat mammalian cancer.

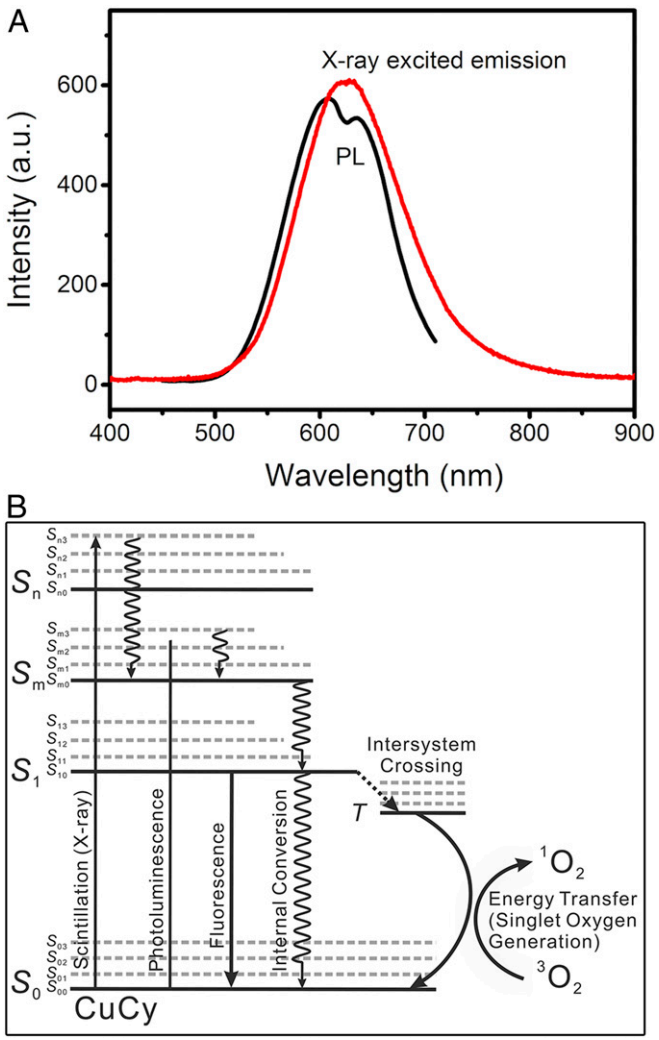

Fig. 4. (*A*) Photoluminescence (PL, excitation at 365 nm) and X-ray–excited luminescence spectra from Cu-Cy nanoparticles. (*B*) Schematic illustration of the scintillation processes in Cu-Cy nanoparticles upon X-ray irradiation. After X-ray irradiation, it may produce photoluminescence, fluorescence, internal conversion, and an intersystem crossing that transfers energy to excite oxygen to produce singlet oxygen.

Materials and Methods

Cu-Cy Nanoparticle Synthesis and Characterization. Cu-Cy nanoparticles were synthesized at The University of Texas at Arlington (56). For size characterization, Cu-Cy nanoparticles dispersed in water were placed on holey carbon-covered copper grids for HRTEM observations. The HRTEM images of the particles were obtained with a Hitachi 9500 electron microscope using an accelerating voltage of 300 kV (55).

Preparation of pHLIP Conjugated Cu-Cy Nanoparticles. Two milligrams of Var3 pHLIP (Ala-28-Gly), from CS Bio Company, was added to 5 mL of deionized water followed by the addition of 3.19 mg of 1 Ethyl-3-(3-dimethylaminopropyl) carbodiimide under mild stirring for 10 min at room temperature. After adjusting the pH to 7.5 using NaOH, 5 mL of 1 mM Cu-Cy nanoparticles (in a water solution) was added under constant stirring overnight at room temperature in a dark environment. The pHLIP-Cu-Cy nanoparticle conjugates were centrifuged at 4,400 rpm for 25 min and washed with deionized water three to four times to remove the precipitates and then were purified by dialysis to remove unreacted species.

Cell Culture. JC Breast murine cancer cells of BALB/cRos strain (CRL-2116) were purchased from American Type Culture Collection and were grown in Roswell Park Memorial Institute (RPMI) medium with L-glutamine and sodium bicarbonate, 10% FBS (Sigma-Aldrich), and 0.1% Ciprofloxacin. The cells were maintained in a humidified atmosphere at 5% carbon dioxide at 37 °C in an incubator. Breast cancer is one example of a cancer type that is reachable at the X-ray energies used in this experiment.

Animal Models and Cell Injection. All animal work followed the guidelines of the University of Rhode Island Institutional Animal Care and Use Committee protocol AN1516-003. Male and female BALB/c mice, 3–4 wk in age, were ordered from Envigo. Male and female mice were used to take the important biological variable of sex into account. For tumor cell inoculation, 1.5 million cells were suspended in 100 mL of RPMI and injected subcutaneously on the right flank of the mice using 1 mL of 27 $G^{1/2}$ latex-free BD syringes.

Radiation Therapy on Mice. Mice were divided into six treatment groups: (*i*) pHLIP-Cu-Cy nanoparticles + radiation; (*ii*) Cu-Cy nanoparticles + radiation; (*iii*) phosphate-buffered saline (PBS) + radiation; (*iv*) pHLIP-Cu-Cy nanoparticles; (*v*) Cu-Cy nanoparticles; and (*vi*) PBS (control). In total, 51 mice (24 males and 27 females) were used for the experiment.

Treatment was undertaken when the tumor size (length) reached ~4–8 mm. Mice were anesthetized using isoflurane gas. For groups of mice given nanoparticles, the nanoparticles were injected intratumorally in 20 μL of PBS at a nanoparticle concentration of 0.8 μg/μL. For the groups given radiation therapy, the mice were irradiated 30 min after injection of particles with an irradiation dose of 5 Gy. Mice were shielded using lead; the only area irradiated was the vicinity of the tumor—the irradiation area was an approximate semicircle 1 inch in diameter. No external X-ray filter was used, and the

source to surface distance was set to 30.5 cm with a field size of 18.3 by 20.1 cm. The current and voltage settings of the X-ray machine (Faxitron MultiRad 350) were 90 kVp and 30 mA, respectively. The nonirradiated mice were also placed in the X-ray chamber, with the same settings except no radiation was given. The tumor size was measured daily using digital Vernier calipers (VCD001, from United Scientific Supply) to get the tumor volume. The tumor volume was calculated using the formula tumor volume = 1/2 length × width^2 (62). Mice were euthanized if they reached or approached the endpoint tumor length of 20 mm, the tumors were necrosed, or if the mice showed signs of distress. Nine mice were euthanized before these endpoints were reached (between days 57 and 93 after irradiation); one mouse was found dead during the experiment.

For tumor targeting with pHLIP, pHLIP-conjugated Cu-Cy nanoparticles should be injected intravenously (i.v.) instead of intratumorally. As a first step, intratumoral injections were used to more accurately compare these results with previous work (46). After this study, i.v. injections will be evaluated in future work.

Statistics and Analysis of Data. In total, 51 mice were used: 24 males and 27 females. Each of the radiation therapy groups had three males and four females, whereas the nonradiation therapy groups had five males and five females. Given that the data are longitudinal with follow-up truncated by death (63), a joint model of longitudinal (cube root of daily tumor volume) and survival response (time to death) was applied to assess the longitudinal trajectory effect of each treatment and its impact on survival simultaneously while controlling for contributing baseline and demographic factors. The effects of baseline (tumor size at irradiation) and demographic (sex and estimated age at irradiation) factors were controlled by including those factors as independent variables/covariates in the joint model. The cube root of volume was used as a measure of tumor size (64, 65). This approach is similar to the concept of the geometric mean of the tumor size (cubic root of length times width times height; ref. 66), although the tumor height was not measured here.

A mixed-effects regression model was assumed for the longitudinal data, and a Cox proportional hazards model was assumed for the survival data. To induce the correlation between longitudinal and survival response, we further assumed the mixed-effects regression model and the hazard function of Cox model shared the same quadratic time trajectory function (67). The covariates considered in both longitudinal and survival models include sex, radiation, treatment effects (no nanoparticles, pHLIP-Cu-Cy nanoparticles, and Cu-Cy nanoparticles), interaction effects between radiation and treatment, age at irradiation, and tumor size at irradiation (cube root of volume). Multiple comparisons between different treatments were also conducted. *P* values from multiple comparisons were corrected by the FWER approach. All analyses were run in SAS version 9.4 using JMFit SAS macro.

ACKNOWLEDGMENTS. Research reported in this publication was supported by the Institutional Development Award Network for Biomedical Research Excellence from the National Institute of General Medical Sciences of the NIH under Grant P20GM103430. M.P.A. also acknowledges the support of startup funds from the University of Rhode Island. W.C. acknowledges the support from the US Army Medical Research Acquisition Activity under Contracts W81XWH-10-1-0279 and W81XWH-10-1-0234 as well as the partial support from NIH/National Cancer Institute Grant 1R15CA199020-01A1. J.W. acknowledges the start-up support from the University of Rhode Island.

1. M. AlSalhi, M. Atif, A. Alobiadi, A. Aldwayyan, A study of the photodynamic effect on cancerous cells. *Laser Phys. Lett.* **9**, 611–617 (2012).
2. S. B. Brown, E. A. Brown, I. Walker, The present and future role of photodynamic therapy in cancer treatment. *Lancet Oncol.* **5**, 497–508 (2004).
3. A. M. Bugaj, Targeted photodynamic therapy–A promising strategy of tumor treatment. *Photochem. Photobiol. Sci.* **10**, 1097–1109 (2011).
4. A. P. Castano, P. Mroz, M. R. Hamblin, Photodynamic therapy and anti-tumour immunity. *Nat. Rev. Cancer* **6**, 535–545 (2006).
5. C.-K. Lim *et al.*, Nanophotosensitizers toward advanced photodynamic therapy of cancer. *Cancer Lett.* **334**, 176–187 (2013).
6. L. Ma *et al.*, X-ray excited ZnS: Cu, Co afterglow nanoparticles for photodynamic activation. *Appl. Phys. Lett.* **105**, 013702 (2014).
7. A. Master, M. Livingston, A. Sen Gupta, Photodynamic nanomedicine in the treatment of solid tumors: Perspectives and challenges. *J. Control. Release* **168**, 88–102 (2013).
8. J. Moan, Q. Peng, An outline of the hundred-year history of PDT. *Anticancer Res.* **23**, 3591–3600 (2003).
9. B. C. Wilson, M. S. Patterson, The physics, biophysics and technology of photodynamic therapy. *Phys. Med. Biol.* **53**, R61–R109 (2008).
10. T. J. Dougherty *et al.*, Photodynamic therapy. *J. Natl. Cancer Inst.* **90**, 889–905 (1998).
11. W. M. Sharman, C. M. Allen, J. E. van Lier, Photodynamic therapeutics: Basic principles and clinical applications. *Drug Discov. Today* **4**, 507–517 (1999).
12. W. Chen, J. Zhang, Using nanoparticles to enable simultaneous radiation and photodynamic therapies for cancer treatment. *J. Nanosci. Nanotechnol.* **6**, 1159–1166 (2006).
13. G. Palumbo, Photodynamic therapy and cancer: A brief sightseeing tour. *Expert Opin. Drug Deliv.* **4**, 131–148 (2007).
14. D. K. Chatterjee, L. S. Fong, Y. Zhang, Nanoparticles in photodynamic therapy: An emerging paradigm. *Adv. Drug Deliv. Rev.* **60**, 1627–1637 (2008).
15. E. J. Hong, D. G. Choi, M. S. Shim, Targeted and effective photodynamic therapy for cancer using functionalized nanomaterials. *Acta Pharm. Sin. B* **6**, 297–307 (2016).
16. N. L. Oleinick, H. H. Evans, The photobiology of photodynamic therapy: Cellular targets and mechanisms. *Radiat. Res.* **150** (suppl. 5), S146–S156 (1998).
17. J. Hu *et al.*, Nanocomposite-based photodynamic therapy strategies for deep tumor treatment. *Small* **11**, 5860–5887 (2015).
18. R. R. Allison *et al.*, Photosensitizers in clinical PDT. *Photodiagn. Photodyn. Ther.* **1**, 27–42 (2004).
19. N. M. Bleehen, J. M. Ford, Radiotherapy, hyperthermia, and photodynamic therapy for central nervous system tumors. *Curr. Opin. Oncol.* **5**, 458–463 (1993).
20. D. E. Dolmans, D. Fukumura, R. K. Jain, Photodynamic therapy for cancer. *Nat. Rev. Cancer* **3**, 380–387 (2003).
21. G. C. Dong, S. X. Hu, G. Y. Zhao, S. Z. Gao, L. R. Wu, Experimental study on cytotoxic effects of hyperbaric oxygen and photodynamic therapy on mouse transplanted tumor. *Chin. Med. J. (Engl.)* **100**, 697–702 (1987).
22. S. Evrard, M. Aprahamian, J. Marescaux, Intra-abdominal photodynamic therapy: From theory to feasibility. *Br. J. Surg.* **80**, 298–303 (1993).
23. A. M. Batlle, Porphyrins, porphyrias, cancer and photodynamic therapy–A model for carcinogenesis. *J. Photochem. Photobiol. B* **20**, 5–22 (1993).
24. B. Bui, L. Liu, W. Chen, Latex carrier for improving protoporphyrin IX for photodynamic therapy. *Photodiagn. Photodyn. Ther.* **14**, 159–165 (2016).
25. H. Chen *et al.*, Nanoscintillator-mediated X-ray inducible photodynamic therapy for in vivo cancer treatment. *Nano Lett.* **15**, 2249–2256 (2015).
26. C. Wang, L. Cheng, Z. Liu, Upconversion nanoparticles for photodynamic therapy and other cancer therapeutics. *Theranostics* **3**, 317–330 (2013).
27. W. Chen, Nanoparticle self-lighting photodynamic therapy for cancer treatment. *J. Biomed. Nanotechnol.* **4**, 369–376 (2008).
28. D. Bechet *et al.*, Nanoparticles as vehicles for delivery of photodynamic therapy agents. *Trends Biotechnol.* **26**, 612–621 (2008).
29. A. Feofanov *et al.*, Near-infrared photosensitizer based on a cycloimide derivative of chlorin p6: 13,15-N-(3′-hydroxypropyl)cycloimide chlorin p6. *Photochem. Photobiol.* **75**, 633–643 (2002).
30. J. P. Rovers, M. L. de Jode, M. F. Grahn, Significantly increased lesion size by using the near-infrared photosensitizer 5,10,15,20-tetrakis (m-hydroxyphenyl)bacteriochlorin in interstitial photodynamic therapy of normal rat liver tissue. *Lasers Surg. Med.* **27**, 235–240 (2000).
31. J. P. Rovers, M. L. de Jode, H. Rezzoug, M. F. Grahn, In vivo photodynamic characteristics of the near-infrared photosensitizer 5,10,15,20-tetrakis(M-hydroxyphenyl) bacteriochlorin. *Photochem. Photobiol.* **72**, 358–364 (2000).
32. S. Banfi *et al.*, Zinc phthalocyanines-mediated photodynamic therapy induces cell death in adenocarcinoma cells. *J. Organomet. Chem.* **692**, 1269–1276 (2007).
33. N. Brasseur, R. Ouellet, C. La Madeleine, J. E. van Lier, Water-soluble aluminium phthalocyanine-polymer conjugates for PDT: Photodynamic activities and pharmacokinetics in tumour-bearing mice. *Br. J. Cancer* **80**, 1533–1541 (1999).
34. M. L. Anderson *et al.*, Rheed and optical characterization of ordered multilayers of phthalocyanine C60 and phthalocyanine perylene-tetracarboxylicdianhydride (Ptcda). *Surf. Sci.* **307–309**, 551–558 (1994).
35. J. M. Fox *et al.*, Synthesis, self-assembly, and nonlinear optical properties of conjugated helical metal phthalocyanine derivatives. *J. Am. Chem. Soc.* **121**, 3453–3459 (1999).
36. X. Zhang, M. L. Gao, X. X. Kong, Y. P. Sun, J. C. Shen, Build-up of a new type of ultrathin film of porphyrin and phthalocyanine based on cationic and anionic electrostatic attraction. *J. Chem. Soc. Chem. Commun.* 1055–1056 (1994).
37. H. Lepor, Vascular targeted photodynamic therapy for localized prostate cancer. *Rev. Urol.* **10**, 254–261 (2008).
38. O. Mazor *et al.*, WST11, a novel water-soluble bacteriochlorophyll derivative; cellular uptake, pharmacokinetics, biodistribution and vascular-targeted photodynamic activity using melanoma tumors as a model. *Photochem. Photobiol.* **81**, 342–351 (2005).
39. H. Guo, H. Qian, N. M. Idris, Y. Zhang, Singlet oxygen-induced apoptosis of cancer cells using upconversion fluorescent nanoparticles as a carrier of photosensitizer. *Nanomedicine* **6**, 486–495 (2010).
40. B. Ungun *et al.*, Nanofabricated upconversion nanoparticles for photodynamic therapy. *Opt. Express* **17**, 80–86 (2009).
41. C. Wang, H. Tao, L. Cheng, Z. Liu, Near-infrared light induced in vivo photodynamic therapy of cancer based on upconversion nanoparticles. *Biomaterials* **32**, 6145–6154 (2011).
42. Y. Zhang, N. M. Idris, Enhanced photodynamic therapy using NIR-to-visible upconversion fluorescent nanoparticles. *Photodiagn. Photodyn. Ther.* **8**, 158 (2011).
43. B. C. Wilson, Photodynamic therapy for cancer: Principles. *Can. J. Gastroenterol.* **16**, 393–396 (2002).
44. S. Imamura *et al.*, Photodynamic therapy and/or external beam radiation therapy for roentgenologically occult lung cancer. *Cancer* **73**, 1608–1614 (1994).
45. H. I. Pass, Photodynamic therapy in oncology: Mechanisms and clinical use. *J. Natl. Cancer Inst.* **85**, 443–456 (1993).

46. L. Ma, X. Zou, W. Chen, A new X-ray activated nanoparticle photosensitizer for cancer treatment. *J. Biomed. Nanotechnol.* **10**, 1501–1508 (2014).
47. Z. Liu *et al*., Investigation of copper cysteamine nanoparticles as a new type of radiosensitiers for colorectal carcinoma treatment. *Sci. Rep.* **7**, 9290 (2017).
48. M. P. Antosh *et al*., Enhancement of radiation effect on cancer cells by gold-pHLIP. *Proc. Natl. Acad. Sci. U.S.A.* **112**, 5372–5376 (2015).
49. O. A. Andreev *et al*., Mechanism and uses of a membrane peptide that targets tumors and other acidic tissues in vivo. *Proc. Natl. Acad. Sci. U.S.A.* **104**, 7893–7898 (2007).
50. O. A. Andreev, D. M. Engelman, Y. K. Reshetnyak, pH-sensitive membrane peptides (pHLIPs) as a novel class of delivery agents. *Mol. Membr. Biol.* **27**, 341–352 (2010).
51. O. A. Andreev, D. M. Engelman, Y. K. Reshetnyak, Targeting diseased tissues by pHLIP insertion at low cell surface pH. *Front. Physiol.* **5**, 97 (2014).
52. M. M. Zulu, A. J. Lees, Multiple-state emission from ligand-bridged tungsten carbonyl [(OC)5W-L-W(CO)5] complexes. *Inorg. Chem.* **28**, 85–89 (1989).
53. Z. Wang, A. J. Lees, Multiple-state emission and excited-state dynamics of CpRe(CO)2L (L = 3-benzoylpyridine and 4-benzoylpyridine) complexes in fluid and glassy solutions. *Inorg. Chem.* **32**, 1493–1501 (1993).
54. A. Vogler, H. Kunkely, Photoluminescence of tetrameric copper(I) iodide complexes solutions. *J. Am. Chem. Soc.* **108**, 7211–7212 (1986).
55. L. Ma *et al*., A new Cu–cysteamine complex: Structure and optical properties. *J. Mater. Chem. C* **2**, 4239–4246 (2014).
56. P. Suriamoorthy *et al*., Folic acid-CdTe quantum dot conjugates and their applications for cancer cell targeting. *Cancer Nanotechnol.* **1**, 19–28 (2010).
57. L. H. Rashidi, H. Homayoni, X. Zou, L. Liu, W. Chen, Investigation of the strategies for targeting of the afterglow nanoparticles to tumor cells. *Photodiagn. Photodyn. Ther.* **13**, 244–254 (2016).
58. O. J. Dunn, Estimation of the means of dependent variables. *Ann. Math. Stat.* **29**, 1095–1111 (1958).
59. M. A. J. Rodgers, P. T. Snowden, Lifetime of oxygen (O2(1.DELTA.g)) in liquid water as determined by time-resolved infrared luminescence measurements *J. Am. Chem. Soc.* **104**, 5541–5543 (1982).
60. R. W. Redmond, I. E. Kochevar, Spatially resolved cellular responses to singlet oxygen. *Photochem. Photobiol.* **82**, 1178–1186 (2006).
61. D. Grossi Marconi *et al*., Head and neck non-melanoma skin cancer treated by superficial X-ray therapy: An analysis of 1021 cases. *PLoS One* **11**, e0156544 (2016).
62. E. K. Rofstad, T. Brustad, Tumour growth delay following single dose irradiation of human melanoma xenografts. Correlations with tumour growth parameters, vascular structure and cellular radiosensitivity. *Br. J. Cancer* **51**, 201–210 (1985).
63. B. F. Kurland, L. L. Johnson, B. L. Egleston, P. H. Diehr, Longitudinal data with follow-up truncated by death: Match the analysis method to research aims. *Stat. Sci.* **24**, 211 (2009).
64. S. R. Oakes *et al*., Loss of mammary epithelial prolactin receptor delays tumor formation by reducing cell proliferation in low-grade preinvasive lesions. *Oncogene* **26**, 543–553 (2007).
65. R. A. Rendon *et al*., The natural history of small renal masses. *J. Urol.* **164**, 1143–1147 (2000).
66. E. Mandonnet *et al*., Continuous growth of mean tumor diameter in a subset of grade II gliomas. *Ann. Neurol.* **53**, 524–528 (2003).
67. D. Zhang, M. H. Chen, J. G. Ibrahim, M. E. Boye, W. Shen, JMFit: A SAS macro for joint models of longitudinal and survival data. *J. Stat. Softw.* 10.18637/jss.v071.i03 (2016).